Self-Assembled Hydrophobin Protein Films at the Air−Water Interface: Structural Analysis and Molecular Engineering†

Géza R. Szilvay,*,‡,§ Arja Paananen,‡ Katri Laurikainen,‡ Elina Vuorimaa,|| Helge Lemmetyinen,|| Jouko Peltonen,⊥ and Markus B. Linder‡

VTT Technical Research Centre of Finland, P.O. Box 1000, FI-02044 VTT, Espoo, Finland, Programme for Structural Biology and Biophysics, Institute of Biotechnology, University of Helsinki, FIN-00014, Helsinki, Finland, Institute of Materials Chemistry, P.O. Box 541, Tampere University of Technology, FI-33101 Tampere, Finland, and Department of Physical Chemistry, Åbo Akademi University, Porthansgatan 3-5, FIN-20500 Turku, Finland

Received November 14, 2006; Revised Manuscript Received December 22, 2006

ABSTRACT: Hydrophobins are amphiphilic proteins produced by filamentous fungi. They function in a variety of roles that involve interfacial interactions, as in growth through the air−water interface, adhesion to surfaces, and formation of coatings on various fungal structures. In this work, we have studied the formation of films of the class II hydrophobin HFBI from *Trichoderma reesei* at the air−water interface. Analysis of hydrophobin aqueous solution drops showed that a protein film is formed at the air−water interface. This elastic film was clearly visible, and it appeared to cause the drops to take unusual shapes. Because adhesion and formation of coatings are important biological functions for hydrophobins, a closer structural analysis of the film was made. The method involved picking up the surface film onto a solid substrate and imaging the surface by atomic force microscopy. High-resolution images were obtained showing both the hydrophilic and hydrophobic sides of the film at nanometer resolution. It was found that the hydrophobin film had a highly ordered structure. To study the orientation of molecules and to obtain further insight in film formation, we made variants of HFBI that could be site specifically conjugated. We then used the avidin−biotin interaction as a probe. On the basis of this work, we suggest that the unusual interfacial properties of this type of hydrophobins are due to specific molecular interactions which lead to an ordered network of proteins in the surface films that have a thickness of only one molecule. The interactions between the proteins in the network are likely to be responsible for the unusual surface elasticity of the hydrophobin film.

Hydrophobins are surface-active proteins produced by filamentous fungi (*1*, *2*). So far, they have been found in all filamentous fungi, and often several different hydrophobin genes are found. Some of the genes are remarkably highly expressed under certain growth phases. Hydrophobins perform several different tasks in growth and development. For example, they form coatings on spores, hyphae, and fruiting bodies. They can have roles in the attachment of fungi to different surfaces, for example, in pathogen−host interactions (*3*). They also play a role in breaking the surface tension of water to enable the formation of fungal aerial structures (*4*). A common factor for all of these functions seems to be that they all involve various interfacial interactions. Studies on hydrophobins have also shown that they can be extremely efficient in foam formation (*5*).

The surface activity of hydrophobins has been utilized in biotechnical applications. Some hydrophobins partition exceptionally well in aqueous surfactant-based two-phase systems (*6*) and have been used as novel tags for purifying recombinant proteins (*7*). The binding of hydrophobins to surfaces has also been used for immobilization of recombinant fusion proteins to surfaces (*8*).

One distinguishing feature of all hydrophobins is that they have eight conserved Cys residues that form a characteristic pattern in their primary sequence. Sequence alignments and reported functional characteristics of hydrophobins are used to group hydrophobins into two classes, I and II. This grouping is useful in predicting properties of hydrophobins, the main difference being that class I members typically form aggregates that are highly insoluble, whereas the aggregates of class II members dissolve more readily. A remarkable property distinctive to class I proteins is that using the strong acid, trifluoroacetic acid, is one of the few ways to dissolve them. Moreover, after removal of the acid the protein is fully functional again. Of the class I members, the SC3 hydrophobin from *Schizophyllum commune* (*9*−*11*) is probably the most studied.

A structural basis for understanding how hydrophobins function was gained when the high-resolution X-ray structures of hydrophobins of the class II members, HFBI and HFBII from *Trichoderma reesei*, were solved (*12*−*14*). These structures showed that the protein is essentially a large and

† This work was funded by the National Graduate School in Informational and Structural Biology (G.R.Sz.), the Academy of Finland (Grant 205997), Tekes, and VTT.

* Corresponding author. E-mail: Geza.Szilvay@vtt.fi. Tel: +358 20722111. Fax: +358 207227071.

‡ VTT.

§ University of Helsinki.

|| Tampere University of Technology.

⊥ Åbo Akademi University.

10.1021/bi602358h CCC: $37.00
Published on Web 02/13/2007

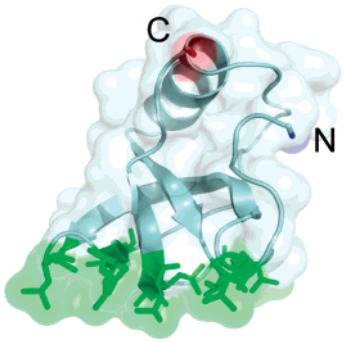

FIGURE 1: X-ray crystal structure of the amphiphilic protein NCys-HFBI [PDB ID 2GVM (*13*, *34*)]. The conserved hydrophobic aliphatic amino acid residues form a planar patch (green). The 11 amino acids in the amino terminus are not visible in the X-ray structure because of mobility of the long linker or protein degradation. The protein variants used in this study had modified termini. Maleimide-PEO_2-biotin was linked either via the 11 amino acid linker to the N-terminus (blue) or directly to the C-terminus (red) as described in the Experimental Procedures. The figure was produced with PyMOL (*35*).

rigid amphiphilic molecule (Figure 1). It has been shown for HFBI that in solution it also behaves in a way analogous to surfactants (*15*). It is very soluble in aqueous solution and forms oligomers in solution in a concentration-dependent manner. The oligomers are in some ways analogous to micelles, however, with the clear difference that the hydrophobin oligomers contain only a finite number of molecules, apparently two or four. The relation between the surface tension reduction and the formation of oligomers in solution is still not completely clear. Initial experiments on interfacial activity showed that the surface affinity of hydrophobins is sufficient to produce compressed films by the Langmuir−Blodgett technique and that nanometer resolution images of the films could be obtained by atomic force microscopy (AFM)[1] (*16*).

Although a model where protein−protein interactions and amphiphilic structures are important components is emerging, there are still several important features that remain to be explained, especially the behavior and self-assembly at interfaces. The investigation of the function of hydrophobins is important for understanding the physiology of fungi and how they interact with their environment. The unique interfacial properties of hydrophobins are also making them increasingly interesting for biotechnological applications and as tools in biochemical research. In this work we describe how the formation of a very unusual elastic surface film was observed and how we were able to use AFM and protein engineering to obtain a structural insight into the features of this film. The results offer a new way of understanding the origin of the extraordinary interfacial properties of hydrophobins.

EXPERIMENTAL PROCEDURES

Site-Directed Mutagenesis, Protein Production, and Purification. HFBI was produced and purified as described previously (*16*). Two different engineered HFBI variants, NCys-HFBI and HFBI-CysC, with single thiol groups added were used in this study. The production and purification of NCys-HFBI, which has an additional cysteine at the N-terminal of the protein, have been described previously (*15*). The other variant, HFBI-CysC, was designed to have an additional cysteine at the C-terminal of the protein. The *hfb1* gene in the plasmid pGZ7 (*15*) was modified using the QuikChange site-directed mutagenesis kit (Stratagene) to yield an *hfb1* variant with the amino acid sequence FCT insertion before the stop codon, resulting in the plasmid pGZ10AC. The oligonucleotides used were CCGCCGTCGG TGCTTTCTGT ACCTGAGGAT CCCCCGGG (sense) and CCCGGGGGAT CCTCAGGTAC AGAAAGCACC GACGGCGG (antisense) (ordered from Sigma-Genosys Ltd.). The underlined sequence codes for the amino acid sequence FCT before the stop codon. The modified *hfb1* gene was transferred back into the pMQ121 (*6*) vector as a *Bam*HI−*Sac*II (New England Biolabs) fragment to yield pGZ13. The expression cassette containing the modified hydrophobin gene, under the control of *cbh1* regulatory sequences, was released using *Eco*RI and *Sph*I (New England Biolabs). This expression cassette was then cotransformed with pToC202 (acetamide resistance) into the *T. reesei* Rut-C30 Δ*hfb2* strain VTT-D-99676 (*17*, *18*), essentially as described in ref *19*. Shake flask cultivation was made to test the transformants for high HFBI-CysC production with slot blotting and Western blotting using standard protocols. The strain selected for protein productions was termed VTT-D-061176. The protein production and purification were made as for NCys-HFBI, described in ref *15*.

Chemical Conjugation. After protein purification, both NCys-HFBI and HFBI-CysC were in an oxidized, covalent dimeric form via the introduced sulfhydryl group. Before conjugation with biotin, this disulfide was selectively reduced with 50 mM dithiothreitol (Sigma-Aldrich Chemie GmbH) as described previously (*15*). The dithiothreitol-treated proteins were conjugated with maleimide-PEO_2-biotin (Pierce) at pH 7 according to the manufacturer's instructions. Reversed-phase chromatography was used to separate any nonreacted biotin label from the protein solution. Matrix-assisted laser desorption ionization/time-of-flight analysis (Institute of Biotechnology, University of Helsinki, Finland) showed a major peak at *m*/*z* 9205.8 for NCys-HFBI and *m*/*z* 8412.4 for HFBI-CysC. These values correspond well with the calculated masses of the conjugates biotin-NCys-HFBI (9202.3 g·mol^{-1}) and HFBI-CysC-biotin (8409.5 g·mol^{-1}). Protein concentration was determined with analytical reversed-phase high-performance chromatography (HPLC).

Hydrophobins at an Air−Water Interface of a Solution Drop. Hanging drops and sessile drops of HFBI dissolved in water were analyzed with an optical surface tension meter CAM 200 and axisymmetric drop shape analysis software (KSV Instruments).

Preparation of Protein Films. Three different methods were used for producing hydrophobin films: the drop-surface transfer, the Langmuir−Blodgett (LB), and the Langmuir−Schaefer (LS) methods. The samples referred to as "drop-surface films" were made by first allowing a drop of hydrophobin solution to take the shape as shown in Figure 2G. A 100 or 200 μL drop of 10 μg·mL^{-1} hydrophobin solution in buffer (100 mM sodium phosphate and 150 mM sodium chloride at pH 7.0) was placed on Parafilm M (American National Can) and incubated for 1−3 h in ambient

[1] Abbreviations: AFM, atomic force microscopy; HOPG, highly oriented pyrolytic graphite; LB, Langmuir−Blodgett; LS, Langmuir−Schaefer; QCM, quartz crystal microbalance.

conditions or overnight in a humid environment. The film on the top of the surface was then transferred to a 10 mm × 10 mm square piece of freshly cleaved highly oriented pyrolytic graphite (HOPG, ZYA quality) (NT-MDT) by touching the drop's surface with the substrate (Figure 3). The two latter types of films, LB and LS, were used as controls and were prepared using a KSV Minitrough Langmuir trough (KSV Instruments) by spreading 300 μL of a 25 μM hydrophobin protein solution dissolved in water on the subphase consisting of plain buffer (1 mM sodium acetate buffer at pH 5.0) or buffer containing 12 nM avidin (Sigma). Compression of the protein monolayer was started after the surface pressure had been stabilized for 20−30 min. The samples were compressed at a barrier speed of 450 mm^2/min to the deposition pressure of 20 $mN{\cdot}m^{-1}$. The formed hydrophobin monolayer at the air−water interface was then transferred to a solid support to enable AFM imaging. LS films were transferred to HOPG by bringing the substrate horizontally into contact with the protein at the air−water interface. LB films on freshly cleaved mica were prepared as described in ref *16*.

The drop-surface and LS films on HOPG were carefully rinsed five times with 30 μL of buffer to wash away any soluble hydrophobins present in the bulk solution that was carried along from the sample solution. We noticed that unwashed samples were difficult to image with AFM in buffer, since the proteins from the bulk solution seemed to contaminate the AFM tip. The LS and drop-surface film samples were kept under buffer prior to AFM imaging. The LB samples did not adhere on the hydrophilic mica surface during imaging in liquid. Therefore, the LB samples were dried in a vacuum desiccator after sample preparation and imaged with AFM in dry state.

Atomic Force Microscopy. A NanoScope IIIa Multimode AFM ("E" scanner; Digital Instruments/Veeco) was used for imaging the hydrophobin films. The LB film of HFBI was imaged in ambient conditions; the imaging parameters are described in ref *16*. The LS and drop-surface films were imaged in liquid, and the measurements were performed either in water or in buffer (100 mM sodium phosphate and 150 mM sodium chloride at pH 7.0). Avidin was added to the samples by injecting 10 μL of avidin solution (0.1 $mg{\cdot}mL^{-1}$ in buffer) into the AFM liquid imaging cell, yielding a final avidin concentration of about 20 $\mu g{\cdot}mL^{-1}$. Imaging was continued after 10 min incubation. In the liquid measurements, silicon nitride cantilevers (NP-S; Veeco), with the force constant of 0.32 $N{\cdot}m^{-1}$, were used for imaging. Topography images were acquired in the tapping mode using scan rates of approximately 1 Hz and applying a force as low as possible (the free amplitude was typically 0.45 V). The damping ratio (set-point amplitude/free amplitude) was typically about 0.7−0.8. For image analysis and calculation of roughness parameters, a NanoScope III offline workstation and the Scanning Probe Image Processor, SPIP (Image Metrology), were used. The image-processing step included only flattening of the acquired images, if not otherwise stated, for removing possible tilt in the image data. Imaging of the hydrophobin films was reproducible. Correlation averaging was done for single-crystalline areas using SPIP to extract the average structure from the image data. The images were first aligned to the same orientation; then a 20 nm × 20 nm section was correlation averaged over the crystalline area. The unit cell dimensions were measured from Fourier transforms of crystalline areas using the SPIP program.

Quartz Crystal Microbalance. An E4 quartz crystal microbalance with dissipation monitoring (QCM) (Q-Sense) was used to study the binding of proteins. Quartz crystals, 5 MHz AT-cut, with polystyrene coating (Q-Sense) were subjected to 300 μL of 5 μM hydrophobin samples in buffer solution (100 mM sodium phosphate and 150 mM sodium chloride at pH 7.0). Avidin (300 μL, 15 μM subunit concentration in buffer) was then introduced to the hydrophobin surface. The crystal surfaces were rinsed thoroughly with buffer after each protein loading. Saturation was ensured by successive loadings of the protein solutions. Adsorption was monitored real time as a decrease in the resonance frequency of the crystal ($-\Delta f$) and by a change in the dissipation energy of the freely oscillating crystal (ΔD). The bound protein mass was calculated from frequency changes between buffer states, before and after the protein sample additions.

RESULTS

Formation of HFBI Films at the Air−Water Interface. Initially an analysis of the lowering of surface tension of water by the HFBI hydrophobin was attempted. This was done by investigating the shape of drops hanging from syringe needles or drops placed on flat surfaces. Hanging drops of hydrophobin solutions were analyzed using axisymmetric drop shape analysis (*20*). It was found that the shape curves of the hanging drop profiles could not be fitted to the Young−Laplace equation using standard methods, since the drop profiles of HFBI hydrophobin solutions had deformed profile appearances after about 15 min (Figure 2A−D). Another atypical property of hydrophobins was noted when analyzing the shape of a drop of hydrophobin solution on a hydrophobic surface. Initially, the drop profile took a rounded shape, but after a while the drop changed shape, forming a planar surface on top. This planar area then grew and resulted in a trapezoid-like profile with a large, remarkably planar surface on top (Figure 2G). At closer inspection of both the flat face of the drop and the pendent drop, it was possible to see a thin film at the water surface. Especially, if the liquid was disturbed, small wrinkles in the film could be observed (Figure 2J,K).

Structural Analysis of Surface Films Using AFM. It was noted that the surface film present in drops like that shown in Figure 2G could be transferred onto a flat hydrophobic solid surface by simply bringing it into contact with the flat surface of the drop (Figure 3). HOPG was found to be a suitable surface to transfer the hydrophobin film onto because it is nonpolar and its surface is atomically flat over sufficiently large areas, which is required for high-resolution AFM imaging. In this way, the protein layer was deposited onto the hydrophobic graphite surface with the hydrophobic side to the graphite and the hydrophilic side of the protein layer facing outward from the surface. The attachment of proteins to graphite was strong enough to allow washing away any possible hydrophobin present in the bulk solution that was carried along with the water drop. The hydrophobin film on graphite could be seen as a hydrophilic spot when washing the otherwise hydrophobic graphite surface. Because the hydrophilic protein spot was effectively wetted, it could

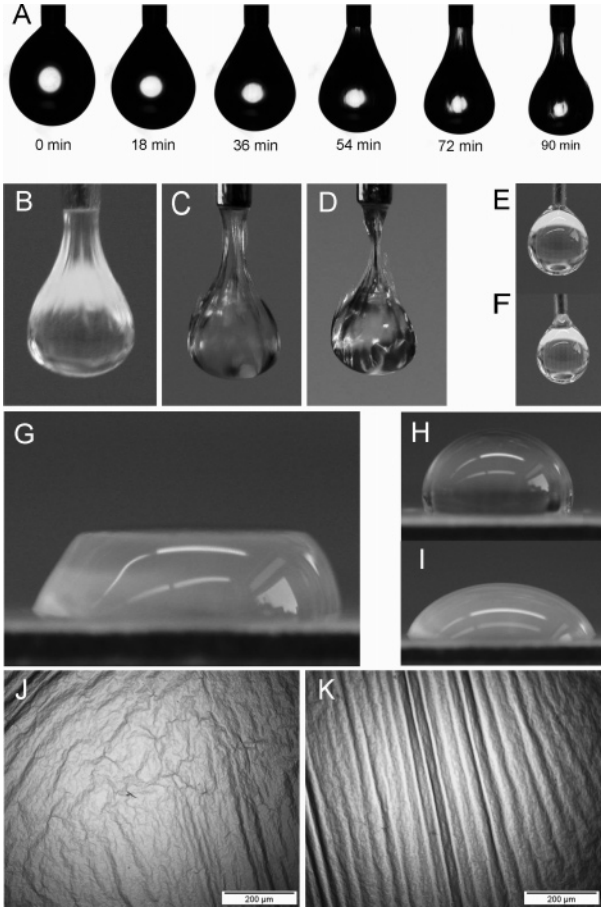

FIGURE 2: Macroscopic effects of HFBI film formation. (A) Pendant drop profile shapes of 100 $\mu g \cdot mL^{-1}$ HFBI in water. Hanging drops of (B) 10 $\mu g \cdot mL^{-1}$ HFBI after 60 min and (C) 100 $\mu g \cdot mL^{-1}$ HFBI after 90 min and (D) 105 min. Hanging drops of (E) water and (F) 1 $mg \cdot mL^{-1}$ sodium dodecyl sulfate. (G) A 50 μL drop of 10 $\mu g \cdot mL^{-1}$ HFBI on a hydrophobic solid after 30 min in ambient environment. Sessile drops of (H) water and (I) 1 $mg \cdot mL^{-1}$ sodium dodecyl sulfate. (J, K) Bright field microscope images of the drop surface of (G).

be kept wet and transferred to the liquid cell of the AFM directly for imaging in buffer without drying in between.

The hydrophobin films that were picked up from flattened drops are referred to here as drop-surface films. For comparison, we also made hydrophobin films using a Langmuir trough (see Experimental Procedures). Films picked up on graphite, in the same way as the drop-surface films, but in which the film had been compressed in a Langmuir trough are called LS films, and films that had been deposited by transferring a hydrophilic substrate (mica) vertically upward through the floating protein monolayer are called LB films. AFM imaging of the HFBI drop-surface and Langmuir hydrophobin interfacial films revealed a regular ordered pattern of objects with the dimension of a few nanometers (Figure 4). In most samples there were raft-like areas with highly ordered structure. In between the highly ordered rafts there were areas with no apparent ordered structure. It is possible that originally larger crystalline domains broke down to smaller ones during film transfer onto the solid supports.

Analyzing the structured parts of the surface using Fourier transforms yielded the dimensions of the basic repeating pattern, which was found to be close to hexagonal in all cases. The results are summarized in Table 1. Film thicknesses were measured from multiple images and samples as a height difference from the substrate to the top of the protein layer. The thickness measurements were enabled by defects of varying sizes in the hydrophobin films. The obtained thicknesses of the LB film, LS film, and drop-surface film were 1.3 ± 0.2, 2.8 ± 0.2, and 2.0 ± 0.2 nm, respectively. The drop-surface films of HFBI had only small defects between the crystalline and amorphous areas, and the AFM tip may not have reached the bottom of the holes; hence the measured thickness is likely to be an underestimation. The HFBI protein itself is close to globular and has a diameter of 2−3 nm according to the X-ray crystal structure (*13*). The value is very close to the measured LS film thickness, and thus the protein film on the drop is most likely to be composed of a monomolecular layer of HFBI. The LB samples were dried before imaging, which very likely explains the lower thickness value.

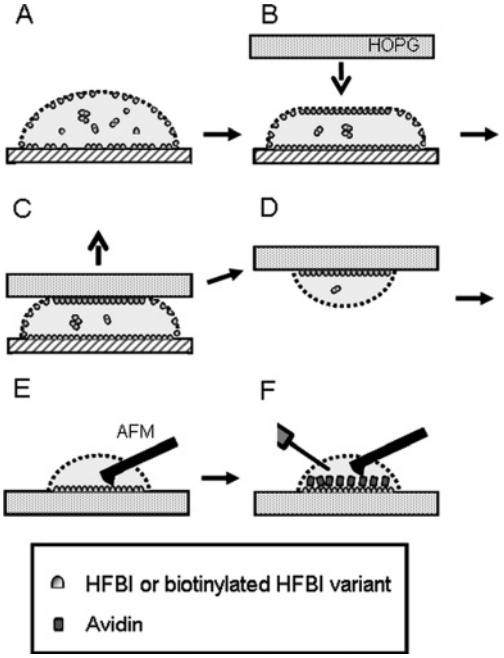

FIGURE 3: Schematic representation of the drop-surface transfer onto a graphite substrate (HOPG). (A) HFBI or biotinylated HFBI variants in water placed as a drop on a hydrophobic solid. (B) The profile of the drop changes shape after about 30 min. (C, D) A HOPG substrate is brought into contact with the drop's surface and lifted up together with the bound protein film. Some liquid is carried along on the HOPG, and the surface is carefully washed (not shown). (E) The sample is imaged in buffer with AFM. (F) Avidin is injected into the AFM liquid cell, and the avidin binding to biotinylated HFBI variants is observed with AFM topography imaging.

The obtained unit cell vector dimensions deviate from a pure hexagonal packing (where $a = b$ and $\gamma = 120°$) (Table 1). Furthermore, there are differences in the unit cells among the different samples. These differences can be explained by scanner hysteresis, creep and drift in the AFM, which become more dominant when capturing images with relatively slow scan speeds. However, despite the distortion caused by the imaging conditions, the lattice constants obtained from the AFM images are very similar in dimensions. The radius of curvature and shape of the tip also influence the topography when imaging small structural features at molecular resolution. Due to differences in tip shapes and sizes sometimes only a little of the periodicities

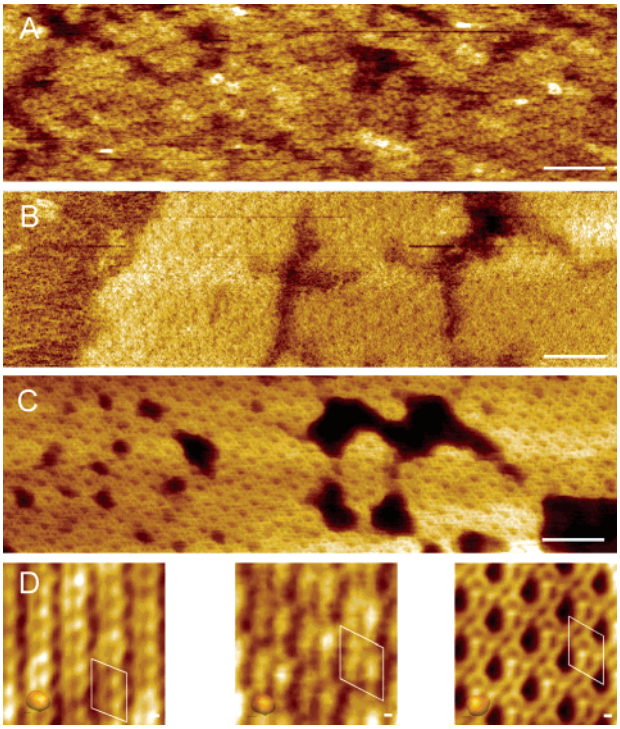

FIGURE 4: AFM topography images of HFBI films: (A) drop-LS film, (B) LS film, and (C) LB film (scale bars are 20 nm). Panels A and B are imaged in buffer, and panel C is imaged in air. (D) Correlation averages of single crystalline areas of (A) (left), (B) (middle), and (C) (right) (scale bars are 1 nm). The unit cells are shown as white parallelograms. For comparison, the structures of HFBI monomers (PDB ID 2FZ6) are shown in scale as insets in the lower left corners of the panels in (D). The low-resolution surface structure of the HFBI monomer was produced using the UCSF Chimera package from the Resource for Biocomputing, Visualization, and Informatics at the University of California, San Francisco (supported by NIH Grant P41 RR-01081) (*36*).

Table 1: Hydrophobin Film Lattice Constant Vectors[a]

protein	film transfer method	a (nm)	b (nm)	γ (deg)
HFBI	LB film	6.07	5.05	119.5
HFBI	LS film	6.11	6.61	125.6
HFBI	drop-surface film	5.92	4.31	116.8
biotin-NCys-HFBI	LS film[b]	5.50	5.65	119.0
HFBI-CysC-biotin	LS film	6.43	5.81	126.1
hexagonal lattice		$a = b$	$b = a$	120

[a] Obtained from Fourier transforms of AFM images. [b] Dry sample.

of the hydrophobin lattice could be seen in the images, but occasionally even 1 nm resolution was achieved. The finer details in the AFM images are most probably brought forth by a possible "microasperity" on the tip surface that actually scans the surface.

Probing the Hydrophobin Film Using Engineered Protein Variants. The initial findings described above strongly suggested that the patterns observed by AFM were ordered assemblies of hydrophobin molecules connected to each other by lateral interactions and with the hydrophobic face of the protein attached to the graphite surface. To verify this and to learn more about the orientation of the proteins, we used protein engineering to make structural variants of HFBI. The strategy to do this was to add a single Cys residue to the hydrophobin and label the introduced sulfhydryl group specifically with biotin. Binding of avidin to the biotin could then be used to probe the position of the biotin molecule,

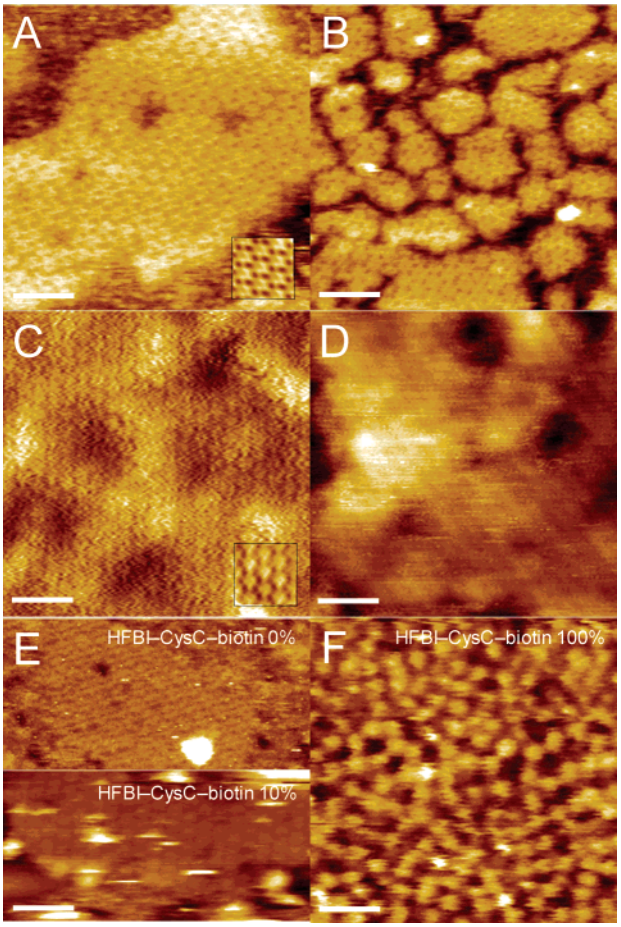

FIGURE 5: AFM topography images of (A−C) biotinylated HFBI variants with (D−F) avidin. (A) HFBI-CysC-biotin LS sample and (B) drop-surface film sample. (C) Biotin-NCys-HFBI dried LS sample. Small insets are correlation averaging results (in scale). The crystalline areas of (B) were too small for reliable correlation averaging. (D) LB sample on mica of biotin-NCys-HFBI incubated with avidin in a Langmuir trough. Here the hydrophobic protein surface is facing upward. (E) Avidin incubated with the (upper part) drop-surface film sample of HFBI and (lower part) LS hydrophobin sample of HFBI-CysC-biotin mixed with HFBI in a ratio of 1:10. (F) Avidin incubated with a drop-surface film sample of HFBI-CysC-biotin. Scale bars are 20 nm.

taking advantage of the possibility to do the probing in situ using the liquid cell of the AFM.

Analyzing the high-resolution X-ray crystal structure of HFBI (*13*) showed that both the N- and C-termini are located near each other at the hydrophilic side of the protein, and conjugation to either one could be feasible. Comparing the sequences of hydrophobins showed that the length of the N-terminus before the first Cys residue is often variable and that the N-terminus of HFBI is, for example, longer than that of the closely related HFBII. Because more variation is allowed in the N-terminus, additions there would be less likely to disturb the function of the protein. A single Cys residue and an 11 amino acid linker part were therefore genetically engineered to the N-terminus of HFBI, and the resulting variant was named NCys-HFBI. The added Cys residue was conjugated with biotin using maleimide-modified biotin. The functionality of the biotinylated NCys-HFBI was shown by studying film formation with the Langmuir trough (Figure 5) and by studying adhesion to hydrophobic surfaces and subsequent binding of avidin (Figure 6). However, we were not able to reproducibly obtain high-resolution AFM

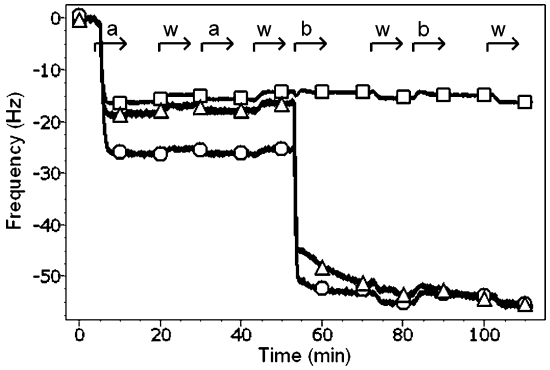

FIGURE 6: QCM measurements of HFBI (squares), biotin-NCys-HFBI (circles), and HFBI-CysC-biotin (triangles) adsorption to polystyrene and the subsequent binding of avidin. All hydrophobins (a) were adsorbed from buffer solution onto the surface. Avidin (b) was introduced to the adsorbed hydrophobin surface. The surfaces were rinsed with buffer (w) after each protein loading.

images of the ordered films of this variant in a liquid environment. Experiments where avidin was added to the liquid chamber showed binding of avidin to the surface as an increase in thickness and a change in surface morphology. Nevertheless, good resolution was obtained when the biotin-NCys-HFBI samples were dried, and the ordered arrangement of the hydrophobin protein was very clearly seen (Figure 5C).

Another variant of HFBI in which the Cys residue was added directly to the C-terminus, called HFBI-CysC, was therefore tested. The C-terminus is located much closer to the core of the protein and not at the end of an extended segment as in the N-terminus. Using the biotin-conjugated form of this variant, it was possible to reproducibly get high-resolution images of the interfacial film on graphite in a liquid environment. It is likely that the extended N-terminal part of the NCys-HFBI variant produces a structure that is flexible and impedes high-resolution imaging in water. The same maleimide−PEO_2 linker that was used for both variants between the protein part and the biotin part apparently did not influence the imaging resolution, as a high imaging resolution was achieved of the HFBI-CysC-biotin sample. The AFM images showed that the formed structures are very similar to native HFBI (Figure 5A−C). The crystal lattices are listed in Table 1.

After imaging the ordered hydrophobin film, avidin was introduced in situ into the AFM liquid cell, and imaging was continued. Avidin was bound to the biotin-functionalized hydrophobin film after about 10 min and covering the hydrophobin film, as seen as an appearance of round avidin-sized objects and an increase in film thickness (Figure 5E,F). Avidin binding was also observed with AFM when the avidin was introduced to the biotin-NCys-HFBI film in the Langmuir trough, before transfer to the graphite substrate with the LS method (data not shown). As expected, no bound avidin was observed in this case on the LB film, that is, on the air-facing side of the air−water interface film (Figure 5D). As the N-terminus of HFBI and hence the conjugated biotin is situated on the hydrophilic side of the protein, the one-sided avidin binding supports the model where the protein's hydrophobic patch is oriented toward the air at the air−water interface. Specificity of the avidin binding was verified with controls using native HFBI. In a buffered environment (100 mM sodium phosphate and 150 mM sodium chloride at pH 7.0), no nonspecific binding to HFBI was observed (Figure 5E, upper part). However, some nonspecific avidin binding to HFBI did occur in pure water (data not shown).

The topography and avidin binding properties of the protein films were further characterized by analyzing 200 nm × 200 nm sized AFM images. The surface characteristics are described by a set of roughness parameters (*21*) calculated for the captured images (Table 2). The root-mean-square roughness S_q for the control sample of HFBI was 0.3 nm. The ten-point-height value (S_z, the average of five lowest minima and five highest maxima) of 3.9 nm is slightly higher than the estimated theoretical diameter of the HFBI protein, most probably because the value includes the nominal roughness of the substrate. The negative skewness (S_{sk}, height asymmetry) value shows that the surface contains holes (valleys). The observed effective surface area (S_{dr} = 15.3%, meaning a surface area being 15.3% larger than that of the projected surface) was surprisingly high when considering the small height differences.

When avidin was introduced onto the control sample, S_q and S_{dr} remained almost constant, referring to no or little adsorbed proteins. The two other parameters, S_z and S_{sk}, show that, indeed, a small amount of avidin was immobilized: those proteins obviously adsorbed nonspecifically by filling the holes of the HFBI film as observed by a less negative skewness value (indicating less holes), simultaneously introducing a slightly increased ten-point-height value.

The introduction of biotin through the engineered Cys residue to the hydrophobin appeared as a slightly increased S_q, indicating a somewhat more heterogeneous structure than that of the films of the reference hydrophobin. Logically, the increased dimensions of the biotin-derivatized hydrophobins led to a film with larger height differences (S_z). However, the height differences were observed to be larger for the derivative with the C-terminated Cys residue, i.e., for the derivative with a shorter biotin−protein linker. The shorter linker might be more upright and stationary than the long linker of the N-terminal modified HFBI, which could be changing positions while imaging. Neither of these surfaces contained holes, as indicated by the positive skewness values. The successful functionality of the biotin groups to bind avidin could be witnessed by adsorption-induced changes in the roughness parameter values. The general roughness (S_q, S_z) increased and the height asymmetry changed, though showing a different trend for the different derivatives. The changes were more pronounced for the N-terminated HFBI, for which, e.g., the effective surface area as a result of avidin binding yielded as high a value as 65.5%. This, however, refers to a rather heterogeneous surface and hence indicates a less effective avidin binding compared with the C-terminated derivative.

Direct Binding of HFBI to Solid Surfaces. Hydrophobin adsorption to polystyrene-coated surfaces and the subsequent binding of avidin were measured with QCM as a change in crystal oscillation frequency. Oscillation dissipation change was always less than one unit, suggesting the formation of a rigid layer. Because the dissipation changes were small relative to frequency change Δf, the amount of adsorbed protein (Δm) on the surface was calculated by the Sauerbrey relation $\Delta m = -C\Delta f/n$, where C = 17.7 ng·Hz^{-1}·cm^{-2}, using the third frequency overtone (n = 3). Adsorption of

Table 2: Roughness Parameters[a]

roughness parameter	parameter name	HFBI	HFBI + avidin	biotin-NCys-HFBI	biotin-NCys-HFBI + avidin	HFBI-CysC-biotin	HFBI-CysC-biotin + avidin
S_q (nm)	RMS roughness	0.3	0.3	0.4	0.9	0.5	0.7
S_{sk}	skewness	−1.24	−0.23	0.12	0.92	3.14	0.86
S_y (nm)	peak−peak height	4.2	5.2	5.3	20.4	6.9	8.3
S_z (nm)	ten point height	3.9	4.9	4.6	12.4	6.5	7.6
S_{dr} (%)	surface area ratio	15.3	16.6	23.0	65.5	12.8	29.7

[a] Calculated from 200 nm × 200 nm sized AFM images.

HFBI and the biotinylated variants, biotin-NCys-HFBI and HFBI-CysC-biotin, to polystyrene was 34.6, 49.6, and 36.2 pmol cm^{-2}, respectively (Figure 6). The amount of avidin binding to the negative control, HFBI, was 0.3 pmol cm^{-2}. Biotin-NCys-HFBI and HFBI-CysC-biotin-coated surfaces bound avidin 8.1 and 9.8 pmol cm^{-2}, respectively. Based on X-ray crystallography structures, the area occupied by a single hydrophobin is about 4 nm^2 and that of an avidin is about 28 nm^2 [PDB IDs 2FZ6 (*13*) and 1AVD (*22*)]. As a rough estimate, the HFBI, biotin-NCys-HFBI, and HFBI-CysC-biotin covered 80%, 120%, and 90% of the surface, respectively, assuming an even layer. Surface coverage of avidin on these hydrophobin layers was respectively 1%, 140%, and 170%. The hydrophobins formed a monolayer as expected. The amount of the estimated avidin bound to the biotinylated hydrophobins was more than a monolayer, probably due to the linker between protein and biotin, which could allow overlapped binding. The HFBI-CysC-biotin seemed to bind more avidin as compared to biotin-NCys-HFBI, a result that was also obtained from the roughness analysis of AFM images. The results show that the biotinylated variants of HFBI behave similarly when bound directly to a solid polymer support as compared to when the hydrophobin layer is picked up from the air−water interface onto a solid support.

DISCUSSION

The aim of this work was to study the behavior of hydrophobins at the air−water interface and to get a structural insight in how the protein organizes itself at the air−water interface. Surface tension is a key parameter in describing the behavior of surface-active agents (surfactants). A common method to determine the surface tension of a liquid is the pendent drop shape analysis, where the shape of a liquid drop, hanging from the tip of a syringe, is analyzed. A drop of pure water will take a close to spherical shape due to its high surface energy, and adding surfactants will make the shape of the drop change due to the lowering of surface tension. The surface tension at the interface can then be derived from the shape of the drop, using a shape factor (*20*). For hydrophobin solutions in ambient conditions, HFBI in this case, the surprising outcome of the experiment was that, while the drop clearly changed shape due to the surface activity, the shape of the drop was such that the shape factor could not be approximated using the numerical tools for solving the Young−Laplace equation that usually are used (Figure 2A). Thus, this commonly used method could not be employed for determining surface activity of hydrophobins. This effect was clearly connected to the spontaneous formation of an elastic-like film at the surface of the drop. A similar, unusual, property of HFBI was also seen when placing a drop of HFBI solution on a flat hydrophobic surface. Upon standing, the top of the drop changed shape from being round-shaped to forming a remarkably shaped drop with a flat top (Figure 2G).

These observations showed that a thin film was formed by HFBI at the air−water interface that had a high coherence and was clearly elastic. These properties make it behave unlike films of typical surfactants. This atypical behavior leads to the questions: what are the structural features of the film and what interactions between hydrophobins are responsible for film formation? To obtain a structural insight in the nature of the hydrophobin films, we developed a method based on liquid-cell AFM that allowed high-resolution imaging of the film in water from the hydrophilic side (Figure 3). This method made it possible to produce images of hydrophobin interfacial films that had never been dried. This is important, because drying of protein samples can cause several artifacts. Drying can, for example, influence the protein structure, and moreover, drying a sample produces at least two interfaces on top of each other, the solid−liquid and the liquid−air. Therefore, it is not necessarily clear which interface really is being investigated. In addition, substances from the bulk liquid are also dried down on the surface.

The results obtained by AFM showed that the film that forms at the air−water interface on a hydrophobin solution drop is one molecule layer thick and has a well-ordered hexagonal-like structure (Figure 4). The results were similar regardless from which side, hydrophobic or hydrophilic, the air−water interface film was analyzed. Surface pressure during film deposition did not seem to affect the lattice constants as seen by comparison of samples compressed to 30 mN/m (*16*) and 20 mN/m (this study). The smallest observable repeating units had a size of about 5 nm, and analysis of these showed that the surface area of each repeating unit was about 20−30 nm^2. Since the hydrophobic patch of HFBI has an area of slightly less that 5 nm^2 (*13*), the hexagonal-like objects are unlikely to represent individual proteins but are rather oligomer-like assemblies. Comparing the AFM image to the structure of monomeric HFBI, we constructed a putative model for the arrangement of individual molecules in the protein film (Figure 7). In the putative arrangement of HFBI molecules on a substrate, the logical assumption is that the hydrophobic patch of the protein is faced toward the graphite (or the air−water interface) and the hydrophilic side toward the aqueous environment (as discussed below). The arrangement can be viewed in two different ways, either as large hexagonal rings consisting of six protein molecules or as an arrangement of oligomers of three molecules in each intersection of a hexagon. The slight deviation of the data and the model is likely to be due to

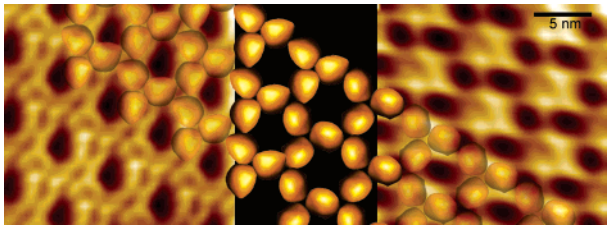

FIGURE 7: Comparison of correlation average AFM images from the HFBI LB sample (left) and HFBI-CysC-biotin LS sample (right) with a suggested model for HFBI arrangement (middle, and extending in both directions). The protein surface representations, generated from the atomic coordinates (PDB ID 2GVM; resolution was reduced using the UCSF Chimera package), are arranged in a suggested hexagon-trimer arrangement and superimposed with the AFM images. The hydrophobin surface representations have their hydrophobic patches facing upward on the left side and downward on the right side of the figure. The biotin-modified HFBI sample (right) was used in the comparison as the hydrophilic side because the best image resolution was obtained from this sample. The ordered structures in the hydrophilic side of HFBI-CysC-biotin and HFBI (Figure 4D, middle) are very similar.

drift in the AFM image, as explained in the Results section. Interestingly, this model would predict the presence of gaps or holes in the framework of the protein. It seems likely that the crystallization of the proteins into the observed regular structure causes the unusual behavior of hydrophobin solution drops. However, it remains unclear what the interactions between the proteins are and how the proteins are positioned in the film.

Another model was previously proposed when no high-resolution structure of any hydrophobin was available (*16*). A low-resolution solution small-angle X-ray scattering model of a HFBI tetramer was compared with AFM images of the HFBI Langmuir film. In that model the repeating units in the HFBI Langmuir film were shown to be of a similar size as multimers formed by HFBI in solution. In the present study we were able to improve the model using the high-resolution X-ray crystal structure of an HFBI monomer.

The variants of HFBI with biotin in either the C- or N-terminus behaved as expected and verified that the patterned surface was made up of HFBI molecules, with their hydrophilic side containing both termini facing toward the solvent. The N- and C-terminal modifications did not notably affect protein functionality. The biotinylated conjugates of both variants exhibited avidin binding in the AFM liquid cell. In addition, they both showed a very similar behavior in the QCM measurements, which suggests that the binding of HFBI to the polystyrene-covered quartz crystal is similar to its assembly at the air−water interface. Avidin binding to biotin (which was attached to the hydrophilic side of the protein) was used to structurally characterize hydrophobin orientation at the air−water interface. Avidin binding was only found on the water-facing side of the biotin-NCys-HFBI film, which confirms the view that at the air−water interface the hydrophilic part of HFBI is facing the water and the hydrophobic part the air. In addition, the experiments show that the hydrophobin membranes can be useful in biotechnology and nanotechnology for investigating individual molecules. The ordered array of protein on surfaces can be useful as a template to tether other molecules in an ordered fashion to the surface: either to study their function or as a step in fabricating devices.

The study of the function of single molecules (or other nanoscale objects) is often hampered by the difficulty to immobilize the object under study to a surface so that the positioning is controlled and oriented. The possibility to image the surface in liquid with AFM additionally has the benefit that solution conditions can be changed and reagents can be added, etc. The experiments also demonstrate how complicated such systems can be. Films of the N-terminally modified protein did not give images with molecular resolution when imaged in liquid, despite several attempts. In contrast, high-resolution images using the C-terminally modified protein were repeatedly obtained. Both types of proteins nonetheless formed similar highly organized layers, since it was possible to obtain high-resolution images of dried samples in air for both samples. Only in liquid did the elongated tail apparently sufficiently disturb the microscopy of the biotin-NCys-HFBI film. Functionally, both variants behaved identically when analyzed using a QCM.

In earlier reports, one of the first indications of self-assembly of hydrophobins was the observation of rodlet layers when drying down drops of the class I hydrophobin SC3 and observing the residue in an electron microscope (*11*, *23*). The produced rods were typically about 10 nm in diameter and hundreds of nanometers in length and packed in bundles in a random way. Freeze fracturing of air vesicles and analysis by electron microscopy showed that rodlets accumulated at the air−water interface (*23*). In more recent studies with SC3 it was concluded that a film described as featureless is produced at low protein concentrations and at short incubation times. Only at higher concentrations and longer incubation times are rodlets formed. The transition of the featureless film into a rodlet film was found to be associated with a secondary structure change in the protein where a transition into a β-sheet state occurred (*9*). The experimental results using class II hydrophobins are clearly different. Neither secondary structure changes nor rodlet layers are observed for HFBI at interfaces (*24*). However, the results of this work suggest that a closer investigation of the featureless film described for SC3 may reveal similarities to the film described here. Rodlet formation may be a result of further interactions occurring in class I hydrophobins but not in class II hydrophobins.

An indication of the structure of hydrophobin films was shown in a previous report (*16*) where HFBI and HFBII at the air−water interface were compressed in a Langmuir trough, lifted from the hydrophilic side on a mica support, and then dried. These LB films showed regularly packed molecules with very similar repeating units than in this study and a film thickness of 1.3 nm. However, drawing conclusions about the function and self-assembly of surfactants based on LB films can be difficult. This is because the compression itself could result in structuring of crystalline films of surfactants as, for example, occurs for cholesterol (*25*). It is therefore not easy to distinguish between ordered structures produced by specific biomolecular interactions and order induced by the compression. Protein 2D crystallization at the air−water interface usually involves protein binding to a preassembled lipid monolayer (*26*−*29*). In some rare examples, however, membrane proteins in lipid bilayers crystallize in vivo in 2D (*30*). In contrast, the 2D crystallization of hydrophobins is a spontaneous process that does not involve the use of lipid layers.

The relatively large size and rigid structure of HFBI and similar hydrophobins make it likely that they will have unusual properties as surfactants. The large area of the hydrophobic patch on the hydrophobin protein surface suggests that the monomer has comparatively high solvation energy (see ref *31*) because a large hydrophobic area is expected to be more efficiently dewetted. However, hydrophobins are very soluble in water. We have shown that this most likely is due to a multimerization behavior in solution that hides the hydrophobic patches from water, in an analogous way as how micelles are formed by typical surfactants (*15*). Experimental data also showed that the protein−protein interactions were dependent on specific structural features of the proteins involved in forming the multimers.

In this work, we show that highly ordered arrangements of hydrophobin are also spontaneously formed at the air−water interface, resulting in a hydrophobin film with elastic properties. Such a 2D arrangement of proteins is expected to involve specific lateral interactions between proteins as well. The combination of a film stabilized by lateral intermolecular forces and amphiphilic structure of the molecules might form synergistically stabilizing effects and explain why the films are so readily formed. We are not currently able to identify the lateral interactions, but they are expected to be located at the hydrophilic sides of the protein. There must therefore be several alternative positions in the hydrophobin molecules where they can interact, depending on if assembly in solution (multimer formation) or at surfaces (2D crystal) is occurring. It is interesting that other forms of assemblies of hydrophobins have been noted, such as readily formed needle-like crystals (*32*). These other assemblies do not have any apparent biological function and may be a fortuitous consequence of the multiple interaction modes that the function of hydrophobins requires.

There are crystallographic data showing dimers and tetramers of HFBI, but trimeric arrangements as suggested in the model shown in Figure 7 have not yet been observed. It is possible that the putative trimer interactions would be specific for the arrangement of hydrophobins at the interface, and a transition from dimer−tetramer to trimer would be associated with film formation.

It is not evident why fungi have evolved to produce hydrophobin-type protein surfactants. However, we can see that the elastic-like films produced by hydrophobins would be very suitable for formation of coatings. The formation of coatings is also believed to be a major biological role of hydrophobins (*2*). The ordered hydrophobin film described in this study may be transferred to the fungal hyphae as the fungus grows through the air−water interface as has been proposed for the rodlet layer of SC3 (*33*).

This system under study gives us the possibility to link structure and architecture at the molecular level to a special functionality at an interface. The use of the avidin−biotin system shows us that both the N- and C-termini are available for binding at the hydrophilic side of the membrane through a short linker and, thus, supports the model presented. Importantly, we also show that this system allows us to use hydrophobins as molecular building blocks for surface engineering. We can see this as a step toward biomolecule-based interface engineering at the molecular level, which was used here for direct AFM imaging of the binding of individual avidin molecules in a native aqueous environment. This example can serve as an excellent model for biomimetic approaches for new applications in interface engineering.

ACKNOWLEDGMENT

We thank Riitta Suihkonen for excellent technical assistance.

REFERENCES

1. Hektor, H. J., and Scholtmeijer, K. (2005) Hydrophobins: proteins with potential, *Curr. Opin. Biotechnol. 16*, 434−439.
2. Linder, M. B., Szilvay, G. R., Nakari-Setälä, T., and Penttilä, M. E. (2005) Hydrophobins: the protein amphiphiles of fungi, *FEMS Microbiol. Rev. 29*, 877−896.
3. Whiteford, J. R., and Spanu, P. D. (2002) Hydrophobins and the interactions between fungi and plants, *Mol. Plant Pathol. 3*, 391−400.
4. Talbot, N. J. (1997) Growing into the air, *Curr. Biol. 7*, 78−81.
5. Sarlin, T., Nakari-Setälä, T., Linder, M., Penttilä, M., and Haikara, A. (2005) Fungal hydrophobins as predictors of the gushing activity of malt, *J. Inst. Brew. 111*, 105−111.
6. Linder, M., Selber, K., Nakari-Setälä, T., Qiao, M., Kula, M.-R., and Penttilä, M. (2001) The hydrophobins HFBI and HFBII from *Trichoderma reesei* showing efficient interactions with nonionic surfactants in aqueous two-phase systems, *Biomacromolecules 2*, 511−517.
7. Linder, M. B., Qiao, M., Laumen, F., Selber, K., Hyytiä, T., Nakari-Setälä, T., and Penttilä, M. E. (2004) Efficient purification of recombinant proteins using hydrophobins as tags in surfactant-based two-phase systems, *Biochemistry 43*, 11873−11882.
8. Linder, M., Szilvay, G. R., Nakari-Setälä, T., Söderlund, H., and Penttilä, M. (2002) Surface adhesion of fusion proteins containing the hydrophobins HFBI and HFBII from *Trichoderma reesei*, *Protein Sci. 11*, 2257−2266.
9. de Vocht, M. L., Reviakine, I., Ulrich, W. P., Bergsma-Schutter, W., Wösten, H. A., Vogel, H., Brisson, A., Wessels, J. G., and Robillard, G. T. (2002) Self-assembly of the hydrophobin SC3 proceeds via two structural intermediates, *Protein Sci. 11*, 1199−1205.
10. Wang, X., Graveland-Bikker, J. F., De Kruif, C. G., and Robillard, G. T. (2004) Oligomerization of hydrophobin SC3 in solution: From soluble state to self-assembly, *Protein Sci. 13*, 810−821.
11. Wösten, H. A., Schuren, F. H., and Wessels, J. G. (1994) Interfacial self-assembly of a hydrophobin into an amphipathic protein membrane mediates fungal attachment to hydrophobic surfaces, *EMBO J. 13*, 5848−5854.
12. Hakanpää, J., Paananen, A., Askolin, S., Nakari-Setälä, T., Parkkinen, T., Penttilä, M., Linder, M. B., and Rouvinen, J. (2004) Atomic resolution structure of the HFBII hydrophobin, a self-assembling amphiphile, *J. Biol. Chem. 279*, 534−539.
13. Hakanpää, J., Szilvay, G. R., Kaljunen, H., Maksimainen, M., Linder, M., and Rouvinen, J. (2006) Two crystal structures of *Trichoderma reesei* hydrophobin HFBI—The structure of a protein amphiphile with and without detergent interaction, *Protein Sci. 15*, 2129−2140.
14. Hakanpää, J., Linder, M., Popov, A., Schmidt, A., and Rouvinen, J. (2006) Hydrophobin HFBII in detail: ultrahigh-resolution structure at 0.75 Å, *Acta Crystallogr., Sect. D: Biol. Crystallogr. 62*, 356−367.
15. Szilvay, G. R., Nakari-Setälä, T., and Linder, M. B. (2006) Behavior of *Trichoderma reesei* hydrophobins in solution: interactions, dynamics, and multimer formation, *Biochemistry 45*, 8590−8598.
16. Paananen, A., Vuorimaa, E., Torkkeli, M., Penttilä, M., Kauranen, M., Ikkala, O., Lemmetyinen, H., Serimaa, R., and Linder, M. B. (2003) Structural hierarchy in molecular films of two class II hydrophobins, *Biochemistry 42*, 5253−5258.
17. Askolin, S., Penttilä, M., Wösten, H. A., and Nakari-Setälä, T. (2005) The *Trichoderma reesei* hydrophobin genes *hfb1* and *hfb2* have diverse functions in fungal development, *FEMS Microbiol. Lett. 253*, 281−288.
18. Bailey, M., Askolin, S., Hörhammer, N., Tenkanen, M., Linder, M., Penttilä, M., and Nakari-Setälä, T. (2002) Process technological effects of deletion and amplification of hydrophobins I

and II in transformants of *Trichoderma reesei*, *Appl. Microbiol. Biotechnol. 58*, 721−727.
19. Penttilä, M., Nevalainen, H., Rättö, M., Salminen, E., and Knowles, J. (1987) A versatile transformation system for the cellulolytic filamentous fungus *Trichoderma reesei*, *Gene 61*, 155−164.
20. Hansen, F. K., and Rødsrud, G. (1991) Surface tension by pendant drop: I. A fast standard instrument using computer image analysis, *J. Colloid Interface Sci. 141*, 1−9.
21. Peltonen, J., Järn, M., Areva, S., Linden, M., and Rosenholm, J. B. (2004) Topographical parameters for specifying a three-dimensional surface, *Langmuir 20*, 9428−9431.
22. Rosano, C., Arosio, P., and Bolognesi, M. (1999) The X-ray three-dimensional structure of avidin, *Biomol. Eng. 16*, 5−12.
23. Wösten, H. A. B., de Vries, O. M. H., and Wessels, J. G. H. (1993) Interfacial self-assembly of a fungal hydrophobin into a hydrophobic rodlet layer, *Plant Cell 5*, 1567−1574.
24. Askolin, S., Linder, M., Scholtmeijer, K., Tenkanen, M., Penttilä, M., de Vocht, M. L., and Wösten, H. A. (2006) Interaction and comparison of a class I hydrophobin from *Schizophyllum commune* and class II hydrophobins from *Trichoderma reesei*, *Biomacromolecules 7*, 1295−1301.
25. Rapaport, H., Kuzmenko, I., Lafont, S., Kjaer, K., Howes, P. B., Als-Nielsen, J., Lahav, M., and Leiserowitz, L. (2001) Cholesterol monohydrate nucleation in ultrathin films on water, *Biophys. J. 81*, 2729−2736.
26. Uzgiris, E. E., and Kornberg, R. D. (1983) Two-dimensional crystallization technique for imaging macromolecules, with application to antigen−antibody−complement complexes, *Nature 301*, 125−129.
27. Scheuring, S., Müller, D. J., Ringler, P., Heymann, J. B., and Engel, A. (1999) Imaging streptavidin 2D crystals on biotinylated lipid monolayers at high resolution with the atomic force microscope, *J. Microsc. 193*, 28−35.
28. Darst, S. A., Ahlers, M., Meller, P. H., Kubalek, E. W., Blankenburg, R., Ribi, H. O., Ringsdorf, H., and Kornberg, R. D. (1991) Two-dimensional crystals of streptavidin on biotinylated lipid layers and their interactions with biotinylated macromolecules, *Biophys. J. 59*, 387−396.
29. Darst, S. A., Ribi, H. O., Pierce, D. W., and Kornberg, R. D. (1988) Two-dimensional crystals of *Escherichia coli* RNA polymerase holoenzyme on positively charged lipid layers, *J. Mol. Biol. 203*, 269−273.
30. Grigorieff, N., Ceska, T. A., Downing, K. H., Baldwin, J. M., and Henderson, R. (1996) Electron-crystallographic refinement of the structure of bacteriorhodopsin, *J. Mol. Biol. 259*, 393−421.
31. Chandler, D. (2005) Interfaces and the driving force of hydrophobic assembly, *Nature 437*, 640−647.
32. Torkkeli, M., Serimaa, R., Ikkala, O., and Linder, M. (2002) Aggregation and self-assembly of hydrophobins from *Trichoderma reesei*: Low resolution structural models, *Biophys. J. 83*, 2240−2247.
33. Wösten, H. A., van Wetter, M. A., Lugones, L. G., van der Mei, H. C., Busscher, H. J., and Wessels, J. G. (1999) How a fungus escapes the water to grow into the air, *Curr. Biol. 9*, 85−88.
34. Berman, H. M., Westbrook, J., Feng, Z., Gilliland, G., Bhat, T. N., Weissig, H., Shindyalov, I. N., and Bourne, P. E. (2000) The Protein Data Bank, *Nucleic Acids Res. 28*, 235−242.
35. DeLano, W. L. (2002) The PyMOL Molecular Graphics System, DeLano Scientific, San Carlos, CA.
36. Pettersen, E. F., Goddard, T. D., Huang, C. C., Couch, G. S., Greenblatt, D. M., Meng, E. C., and Ferrin, T. E. (2004) UCSF Chimera—a visualization system for exploratory research and analysis, *J. Comput. Chem. 25*, 1605−1612.

BI602358H